# Heat transport processes of the Indonesian Throughflow along the outflow pathway in the eastern Indian Ocean during the last 160 kyr

Xuan Ding, Franck Bassinot, Xiaolei Pang, Yingxin Kou, Liping Zhou

Paleoceanography and Paleoclimatology

RESEARCH ARTICLE
10.1029/2023PA004620

**Key Points:**

- Sea surface and thermocline water temperatures and vertical structure of the Indonesian Throughflow (ITF) outflow for the last 160 Kyr were reconstructed
- Vertical structure of the ITF remained unchanged during its penetration into the Indian Ocean
- Variation of the ITF through time impacted the heat transport processes along the outflow pathway in the eastern Indian Ocean

**Supporting Information:**

Supporting Information may be found in the online version of this article.

**Correspondence to:**

X. Ding,
dingx@cugb.edu.cn

**Citation:**

Ding, X., Bassinot, F., Pang, X., Kou, Y., & Zhou, L. (2023). Heat transport processes of the Indonesian Throughflow along the outflow pathway in the eastern Indian Ocean during the last 160 Kyr. *Paleoceanography and Paleoclimatology*, *38*, e2023PA004620. https://doi.org/10.1029/2023PA004620

Received 3 FEB 2023
Accepted 17 AUG 2023



# Heat Transport Processes of the Indonesian Throughflow Along the Outflow Pathway in the Eastern Indian Ocean During the Last 160 Kyr

**Xuan Ding[1,2], Franck Bassinot[3], Xiaolei Pang[4,5], Yingxin Kou[6], and Liping Zhou[4,7]**

[1]School of Ocean Sciences, China University of Geosciences (Beijing), Beijing, China, [2]Key Laboratory of Polar Geology and Marine Mineral Resources (China University of Geosciences, Beijing), Ministry of Education, Beijing, China, [3]LSCE (CEA/CNRS/UVSQ), Domaine du CNRS, Gif-sur-Yvette, France, [4]Institute of Ocean Research, Peking University, Beijing, China, [5]School of Earth and Space Sciences, Peking University, Beijing, China, [6]Research School of Earth Sciences, Australian National University, Canberra, ACT, Australia, [7]Key Laboratory for Earth Surface Processes, Department of Geography, Peking University, Beijing, China

**Abstract** As the only low-latitude connection along the return branch of the Great Conveyor Belt, the Indonesian Throughflow (ITF) plays an important role in the large-scale ocean–atmosphere interaction in the tropical region. However, the heat transport processes of the ITF along the outflow pathway in the eastern Indian Ocean over the recent geologic period is still debated. In this study, by using Mg/Ca ratios of the surface-dwelling and thermocline-dwelling planktonic foraminifera *Globigerinoides ruber* and *Pulleniatina obliquiloculata*, we reconstruct sea surface temperature and thermocline water temperature (TWT), and thermocline structure at two sites in the main outflow path of the ITF in the eastern Indian Ocean for the last 160 Kyr, and compare these new data with those from two cores in the central Indo-Pacific Warm Pool. Our results show that, on the orbital time scale, the thermocline structure changes above the equatorial 90°E Ridge mimic those of the eastern Timor Sea, indicating that the ITF vertical structure remained unchanged during its penetration into the Indian Ocean. The TWT in the equatorial western Pacific and eastern Indian Ocean presents similar change trend, suggesting that the ITF is likely to be an important route for thermocline water transport into the Indian Ocean. However, the vertical structure of the ITF varied through time, reflecting the effects of sea level and orbitally-driven monsoonal activity. This impacted heat transport processes, resulting in changes in the surface water temperature along the outflow pathway in the eastern Indian Ocean.

## 1. Introduction

The transport of surface and subsurface Pacific Ocean water into the Indian Ocean takes place at low latitudes via the Indonesian seas. The current is referred to as the Indonesian Throughflow (ITF) (Gordon, 2005; Gordon et al., 2012) (Figure 1). It is the only low-latitude connection along the return branch of the Great Conveyor Belt, which ultimately brings upper thermocline and surface waters from the Pacific to the North Atlantic (Bray et al., 1996; Gordon, 1986, 2005; Gordon & Fine, 1996; Hirst & Godfrey, 1993; Müller & Opdyke, 2000). Therefore, the ITF plays an important role in large-scale ocean–atmosphere interaction in the tropical region. It modifies the heat and freshwater budgets and air–sea heat fluxes of the Pacific and Indian oceans with potential impacts on the El Niño-Southern Oscillation and Asian monsoon climate (Gordon, 2005; Gordon et al., 2003; Webster et al., 1998). Modern observations made by Gordon (2005) indicated that the ITF cools and freshens the Indian Ocean thermocline. Without the ITF inflow, the low-latitude Indian Ocean thermocline would be warmer, saltier and thicker which would induce warmer tropical sea surface temperatures (SSTs), invigorating the south Asian monsoon. However, our knowledge about the dynamics and evolution of the ITF heat transport in the geological past is still limited.

In recent years, several studies have examined the impacts of tectonically-induced changes in the Indonesian Gateway, sea level changes, Asian monsoon activities, and El Niño–Southern Oscillation on the ITF transport in the western Pacific and Indonesian sea area (Dang et al., 2012; Ding et al., 2013; Fan et al., 2013, 2018; He & Wang, 2021; Holbourn et al., 2011; Linsley et al., 2010; Lückge et al., 2009; Smith et al., 2020; Xu et al., 2006, 2008). Saraswat et al. (2019) expanded investigations into the western regions of the Indian Ocean. They reconstructed the seawater temperature and precipitation changes of the last ~184 Kyr from the southeastern Arabian Sea and attributed the westward extension of the Indo-Pacific Warm Pool (IPWP) during the Marine

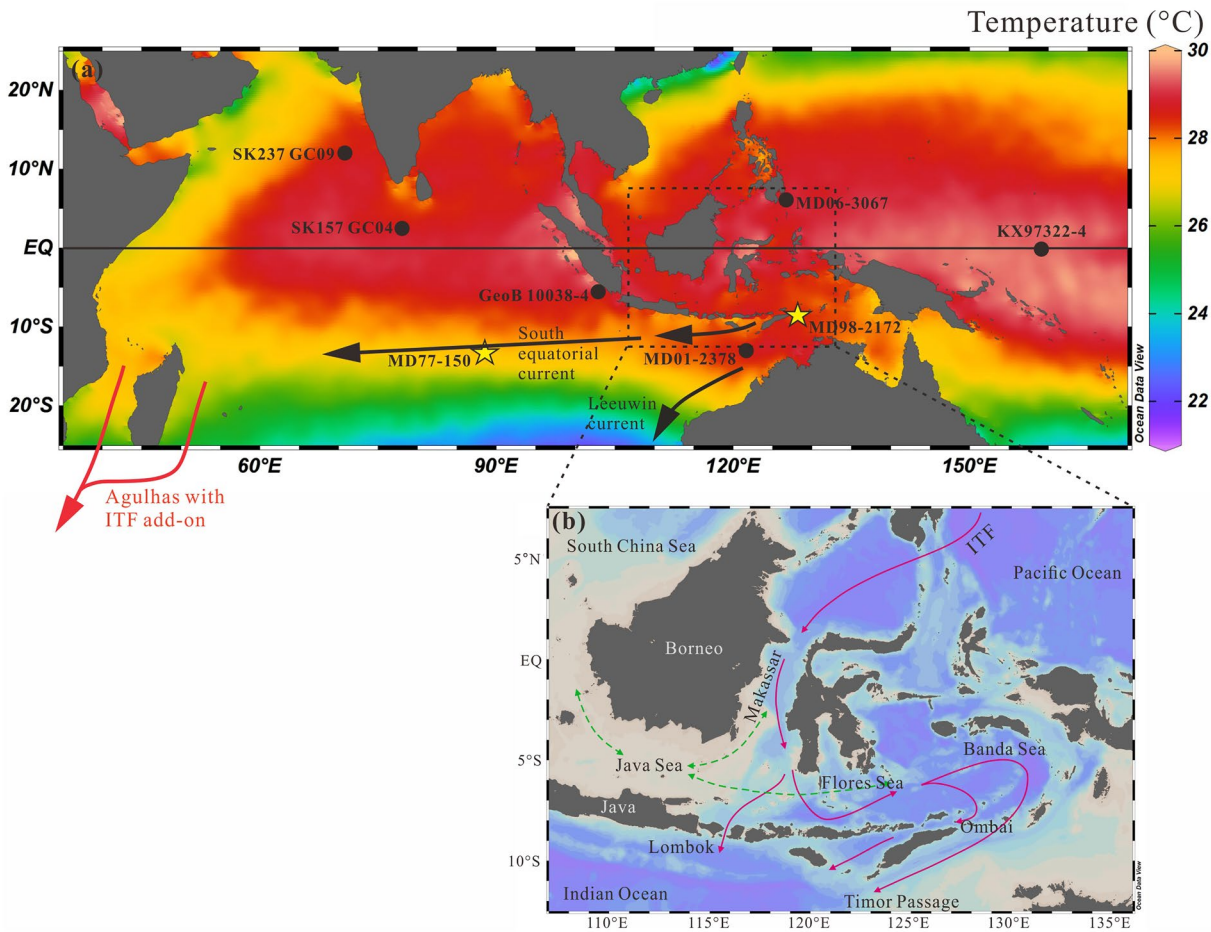


**Figure 1.** (a) Map of annual average SSTs in the Indo-Pacific region based on World Ocean Atlas 2018 data, and locations of the sites MD 98-2172 and MD77-150 and those referred to in the text; (a) (b) Indonesian Throughflow (ITF) pathways in the West Pacific and Indian Oceans (Gordon, 2005; Oppo & Rosenthal, 2010).

Isotope Stages (MIS) 5e and the early Holocene to the transport of warm water to the Indian Ocean through the ITF. This is in contrast to the observations for the same time periods in the Indonesian sea area, which pointed to a dominant cold and fresh thermocline ITF flow (Ding et al., 2013; Xu et al., 2006, 2008).

Present-day observations of the ITF show a watermass structure with clear depth-dependent temperature differences (Gordon et al., 2003; Tozuka et al., 2009). To understand long-term changes in the heat transport processes of the ITF, a major question is then raised regarding past changes in the surface and sub-surface temperatures along the outflow ITF pathway in the eastern Indian Ocean.

The aim of the present study is to characterize the changes of the ITF during the last 160 Kyr and understand their influence on the heat transport processes between the western Pacific and eastern Indian Ocean. Two cores along the main outflow path of the ITF in the eastern Indian Ocean are selected in this study: Core MD98-2172 located in the Timor Sea, and Core MD77-150 on the 90°E Ridge in the equatorial Indian Ocean (Figure 1). We reconstructed past changes of SST and thermocline water temperature (TWT) based on the Mg/Ca-thermometer of the surface-dwelling and thermocline-dwelling planktonic foraminifera *Globigerinoides ruber* and *Pulleniatina obliquiloculata*, respectively, and compared the thermocline structure and temporal evolution at our two study sites with those from the western equatorial Pacific Ocean, which is the core region of the IPWP and the source area of the ITF.

## 2. Oceanography

The main body of the ITF derives from the Mindanao Current of the North Pacific Ocean and most of it travels to the Indian Ocean through the Makassar Strait, with a smaller contribution entering the Indonesian archipelago

through passages located to the west and to the east of Halmahera, and then to the Banda Sea via the Lifamatola Strait (Gordon, 1986; Gordon & Fine, 1996) (Figure 1). The throughflow via the Makassar Strait is limited by the 680 m-deep Dewakang sill, and therefore only the thermocline water enters the Flores Sea. From there, a flux of ∼1.7 Sv of the ITF water directly enters into the Indian Ocean through the shallow (depth of 300 m) Lombok Strait, while the ITF main body turns east to the Banda Sea and enters the Indian Ocean through two main passages, the Ombai Strait (ITF flux ∼ 4.5 Sv) and the Timor Sea (ITF flux ∼ 4.3 Sv) (Gordon, 2005; Gordon & Fine, 1996; Oppo & Rosenthal, 2010; Sprintall et al., 2009) (Figure 1).

The climate of the modern Indonesian seas is dominated by semiannual monsoonal shifts, which are induced by the seasonal latitudinal migration of the Intertropical Convergence Zone (Ardi et al., 2020; Huang et al., 2015; Wang et al., 2012). During the northern hemisphere winter (November–March), the northwest (NW) monsoon is accompanied by heavy rainfall over a large part of Indonesian seas, while the northern hemisphere summer (May–September) induces a southeast (SE) monsoon season with reduced precipitation (Figure 2) (Ardi et al., 2020; Ding et al., 2013; Spooner et al., 2005; Xu et al., 2006).

During the NW monsoon, low-salinity surface water from the Java Sea is advected into the southern Makassar Strait (Figures 2a–2d) and blocks the warm surface ITF flux. During this period, the ITF flux into the Indian Ocean is dominated by the cold thermocline part of ITF. During the SE monsoon period (Figures 2e–2h), the winds blowing over the Java Sea reverse and drive saltier surface water from the Banda Sea into the south Makassar Strait, eliminating the northward pressure gradient. However, the northern SE monsoon over Makassar constrains the surface throughflow (Gordon, 2005). Thus, on a yearly basis the ITF corresponds chiefly to the advection of cool subsurface water in the Indian Ocean, with a smaller contribution of the warm surface flow (Gordon et al., 2003; Tozuka et al., 2009).

Part of the ITF flows southward in the Leeuwin Current along western Australia, but most of the ITF thermocline water entering the Indian Ocean is slowly diluted and mixed with Indian Ocean thermocline waters as it is advected westward within the South Equatorial Current (SEC) and transits across the Indian Ocean (Gordon, 1986; Song et al., 2004). At the African coast, the ITF water passing ultimately along the western boundary through the Mozambique Channel and along the east coast of Madagascar joins the south-flowing Agulhas Current (Figure 1). Part of the Agulhas current turns eastward and recirculates in the Indian Ocean, while a branch rounds the southern tip of Africa and flows into the Atlantic (Gordon, 2005; Gordon et al., 2003; Oppo & Rosenthal, 2010; Song et al., 2004).

## 3. Materials and Methods

### 3.1. Cores Studied

Core MD98-2172 (8°31′S, 128°09′E) was retrieved from the Timor Sea at a water depth of 1,768 m during the International Marine Global Change Study cruise IV of the R/V *Marion Dufresne* (Figure 1). This Calypso giant piston core is 54 m long. Samples from the upper 24 m of the core were taken at 2- to 10-cm intervals for stable isotope analysis of planktonic foraminifera and at 10-cm intervals for planktonic foraminifer census and Mg/Ca measurements.

The paleoceanographic proxy records on the upper 7.5 m of this core (the *G. ruber* $\delta^{18}O$ and $\delta^{13}C$, and the planktonic foraminifera census data) were previously used to analyze the ITF change in the Timor Sea since the last glacial maximum (Ding et al., 2013).

The piston core MD77-150 (12°59′S, 88°28′E) was retrieved on the 90°E Ridge at a water depth of 1,980 m during the cruise OSIRIS3 with the R/V *Marion Dufresne* (Figure 1). Core MD77-150 is 16.5 m in length. We used the upper 2.2 m for this study. Samples were taken at 1-cm intervals for stable isotope analyses and Mg/Ca measurements of planktonic foraminifera.

After being oven-dried at ∼40°C and weighed, samples of the two cores were disaggregated by soaking in water, and then washed through a 63-μm sieve. Residues were collected on filter paper and were oven-dried at 40°C overnight.

### 3.2. Planktonic Foraminiferal Census Counts

For the 7.5–24 m interval of Core MD98-2172, the residues were dry-sieved through a 150-μm sieve, and then split with a micro-splitter to provide a subsample with at least 300 whole tests of planktonic foraminifera which

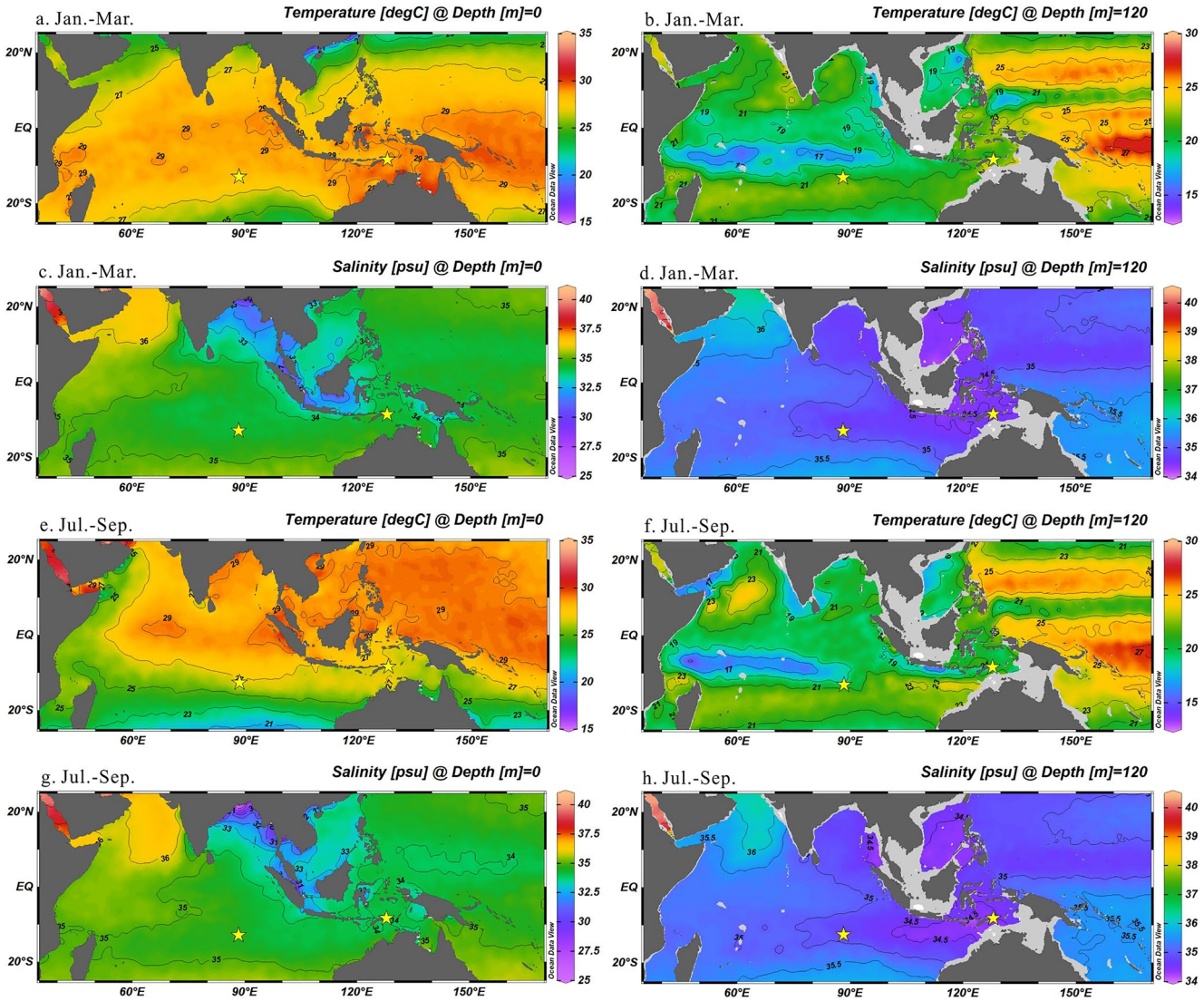


**Figure 2.** Seasonal temperature and salinity distribution in the Indo-Pacific region based on World Ocean Atlas 2018 data. Temperature from January to March at 0 m (a) and 120 m (b); Salinity from January to March at 0 m (c) and 120 m (d); Temperature from July to September at 0 m (e) and 120 m (f); Salinity from July to September at 0 m (g) and 120 m (h). The yellow stars are locations of studied cores MD98-2172 and MD77-150.

were identified and counted. Data were added to the upper 7.5 m initial counts of Ding et al. (2013) to form the record discussed in the present study.

### 3.3. $\delta^{18}O$ and $\delta^{13}C$ Analysis

A total of 10–15 specimens of planktonic foraminifer *G. ruber* in the size range of 250–315 μm were hand-picked for the two cores and then ultrasonically cleaned in methanol for less than 10 s.

For Core MD77-150, stable carbon and oxygen isotopes of planktonic foraminifera were measured on an Element GV mass spectrometer at the Laboratoire des Sciences du Climat et de l'Environnement, Gif-sur-Yvette, France. The external reproducibility is ~0.06‰ for $\delta^{18}O$ (1$\sigma$) and 0.03‰ for $\delta^{13}C$ (1$\sigma$). Isotopic data are reported relative to the Pee Dee Belemnite (PDB) standard through calibration to the NBS 19 standard.

For Core MD98-2172, stable carbon and oxygen isotopes of planktonic foraminifera *G. ruber* picked from the interval 7.5–24 m were measured using a Finnigan MAT-252 mass spectrometer at the State Key Laboratory of Marine Geology, Tongji University, China. The external reproducibility is 0.08‰ for $\delta^{18}O$ (1$\sigma$) and 0.06‰

**Table 1**
*Accelerator Mass Spectrometry $^{14}C$ Dates From Cores MD98-2172 and MD77-150*

| MD98-2172 | | | |
|---|---|---|---|
| Lab code | Sample depth (cm) | $^{14}C$ dates (year BP) | $^{14}C$ cal (year BP) |
| GifA 101513 | 0–2 | 1,330 ± 80 | 815 ± 87 |
| GifA 101512 | 350–351 | 9,120 ± 100 | 9,750 ± 172 |
| GifA 101511 | 418–419 | 11,310 ± 130 | 12,740 ± 122 |
| GifA 101510 | 465–466 | 13,270 ± 290 | 15,242.5 ± 519.5 |
| GifA 101509 | 511–512 | 15,210 ± 180 | 17,934 ± 230 |
| GifA 101508 | 581–582 | 18,250 ± 190 | 21,543.5 ± 269.5 |
| MD77-150 | | | |
| Lab code | Sample depth (cm) | $^{14}C$ dates (year BP) | $^{14}C$ cal (year BP) |
| QAS3001 | 1–2 | 6,005 ± 30 | 6,341.5 ± 43.5 |
| QAS3002 | 4–5 | 6,050 ± 30 | 6,384 ± 52 |
| QAS3604 | 11–12 | 7,770 ± 40 | 8,167 ± 71 |
| QAS3605 | 15–16 | 9,365 ± 45 | 10,143.5 ± 64.5 |
| QAS3606 | 19–20 | 13,200 ± 70 | 15,166.5 ± 114.5 |
| QAS3607 | 31–32 | 19,150 ± 140 | 22,543.5 ± 151.5 |
| QAS3608 | 50–51 | 26,580 ± 360 | 30,335 ± 415 |
| QAS3609 | 60–61 | 30,160 ± 540 | 33,814 ± 527 |
| QAS3610 | 70–71 | 34,520 ± 920 | 38,353.5 ± 1,167.5 |

for $\delta^{13}C$ ($1\sigma$). Isotopic data are reported relative to the PDB standard through calibration to the NBS19 standard.

### 3.4. AMS $^{14}C$ Analysis

Accelerator mass spectrometry (AMS) $^{14}C$ ages were obtained on monospecific samples of *Globorotalia menardii* (>250 μm, ~10 mg) picked from nine intervals for Core MD77-150. The foraminiferal specimens were ultrasonically cleaned in distilled water for 15 s and then submitted for AMS $^{14}C$ dating to the Laboratory for Earth Surface Processes and the Institute of Heavy Ion Physics, Peking University, China. Calendar ages were calculated using the Program Calib 7.10 (http://calib.org/calib/) and the MARINE13 calibration set, applying a modern regional reservoir age correction $\Delta R$ of 71 ± 25 years. The results are given in Table 1.

For Core MD98-2172, the six AMS $^{14}C$ ages from the monospecific samples of *G. ruber* published in Ding et al. (2013) were recalibrated using Calib 7.10 (http://calib.org/calib/) and the MARINE13 calibration set, applying to a modern regional reservoir age correction $\Delta R$ of 59 ± 40 years (Table 1).

### 3.5. Analysis of Mg/Ca Ratios

For the analysis of Mg/Ca ratios, ~40 tests of the planktonic foraminifera surface dweller *G. ruber* (sensu stricto white) and ~30 tests of the upper thermocline dweller *P. obliquiloculata* were picked from size fractions of 250~350 and 350~500 μm, respectively. Samples were gently crushed to expose inner chamber walls, and then transferred into vials for cleaning. The cleaning procedures followed the methods outlined by Barker et al. (2003). They consisted of five water washes and two methanol washes followed by two oxidative steps with a 1% NaOH-buffered $H_2O_2$ and weak acid (0.001 M $HNO_3$) leach and then the samples were dissolved with 0.075M $HNO_3$. After centrifuging for 2 min at 13,000 rpm, samples were transferred to new vials. Mg/Ca ratios were measured using a Varian 715es inductively plasma optical emission spectrometry (ICP-OES) following the intensity ratio method of de Villiers et al. (2002) at the School of Ocean Sciences, China University of Geosciences (Beijing). An external standard solution (Mg/Ca = 4.07 mmol/mol) was measured every six samples to verify the reproducibility. The relative standard deviation is 0.016 mmol/mol (0.4%). Mn/Ca, Al/Ca, and Fe/Ca were also measured for estimating potential contamination by oxyhydroxides or clay material. Samples with high contaminant contents and/or exhibiting a significant correlation between Mn/Ca, Fe/Ca, Al/Ca and Mg/Ca values were excluded.

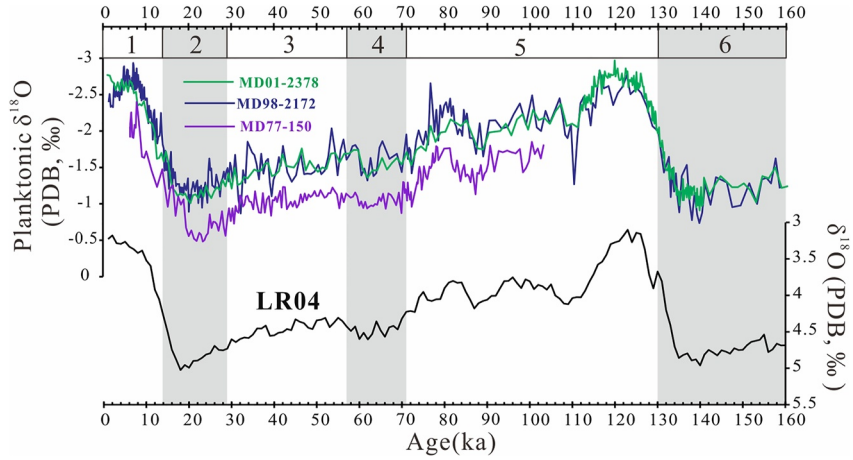


**Figure 3.** Plots of planktonic $\delta^{18}O$ against age in cores MD98-2172 and MD77-150, and MD01-2378 (Holbourn et al., 2005; Xu et al., 2006), stacked LR04 $\delta^{18}O$ curve (Lisiecki & Raymo, 2005). Gray shadings mark the Marine Isotope Stages (MIS) 2, 4, and 6.

Foraminifera Mg/Ca ratios were converted into temperatures using the calibration equations of Anand et al. (2003) for *G. ruber* (250~350 μm): $Mg/Ca = 0.38e^{0.09T}$ and for *P. obliquiloculata*: $Mg/Ca = 0.328e^{0.09T}$.

### 3.6. Calculation of $\delta^{18}O_{sw}$

The surface seawater $\delta^{18}O$ composition ($\delta^{18}O_{sw0}$ VSMOW) was calculated from paired Mg/Ca and $\delta^{18}O$ measurements of *G. ruber* by using the equation of Bemis et al. (1998): $\delta^{18}O_{sw0} = 0.27 + [T(°C) - 16.5 + 4.8\delta^{18}O (VPDB)]/4.8$.

We corrected the ice sheet waxing/waning effect on the $\delta^{18}O_{sw0}$ values using the sea level record of the global ocean (Waelbroeck et al., 2002). The residual oxygen isotope values of seawater ($\delta^{18}O_{sw}$) represent local variations in sea surface salinity (SSS) induced by hydrological changes (evaporation/precipitation) and lateral advection of water.

## 4. Age Models

The age model for the upper 581 cm of Core MD98-2172 was based on six calibrated radiocarbon dates. Below 581 cm, we derived the age model of Core MD98-2172 by visual correlation to the planktonic foraminiferal oxygen isotope record of the nearby Core MD01-2378 (Holbourn et al., 2005; Xu et al., 2006). For this correlation exercise we used the Linage tool of the AnalySeries software (Paillard et al., 1996). Depths were converted to calendar ages by linear interpolation between tie points. The top age of Core MD98-2172 is ~0.8 ka, and the bottom of the studied interval (at 2,404 cm) is set at ~158 ka in MIS 6 (Figure 3).

For Core MD77-150, the age model for the upper 70 cm was based on nine calibrated radiocarbon dates. The age model below 70 cm was derived by visual correlation of planktonic foraminiferal oxygen isotope to that of Core MD98-2172. Depths were converted to calendar ages by linear interpolation between tie points. The top age of the core is ~6.3 ka, indicating that the late Holocene is missing, likely due to the result of incomplete recovery of the top sediments by piston coring. The base of the studied interval, at 219 cm, is set at ~103 ka, which lies within the MIS 5 (Figure 3). AMS $^{14}C$ ages for Core MD77-150 were obtained from planktonic foraminifera sub-surface species *G. menardii*, which may have a potentially larger reservoir age (Stuiver & Braziunas, 1993). Therefore, we compared the oxygen isotope stratigraphic framework of this core with the adjacent Core GeoB 10038-4 (5°56.25′S, 103°14.76′E) from the Mentawai-Basin off west Sumatra (Figure 1) (Mohtadi et al., 2010) to ensure the accuracy of the age model established. The results indicated that the oxygen isotope curves of the two cores show a very consistent trend (Figure S1 in Supporting Information S1).

The average sedimentation rates are ~15.2 cm/Kyr in Core MD98-2172 and ~2.2 cm/Kyr in Core MD77-150. Based on these sedimentation rates, the average temporal resolution for Core MD98-2172 is ~490 years for

planktonic $\delta^{18}O$ and $\delta^{13}C$ records and ~660 years for the Mg/Ca and the planktonic foraminifera census records. For Core MD77-150, the resolution is ~450 years for $\delta^{18}O$, $\delta^{13}C$, and Mg/Ca records.

## 5. Results

### 5.1. $\delta^{18}O$ Record

Over the time interval covered, the $\delta^{18}O$ values of planktonic species *G. ruber* vary between −2.93 and −0.74‰ in Core MD98-2172, and between −2.40 and −0.48‰ in Core MD77-150 (Figure 3). The planktonic $\delta^{18}O$ fluctuations observed in Core MD77-150 on the 90°E Ridge are consistent with those of Core MD98-2172 in the Timor Sea. However, *G. ruber* $\delta^{18}O$ values from Core MD77-150 on the 90°E Ridge are higher by about +0.5‰ PDB on average compared to those from Core MD98-2172 (Figure 3).

### 5.2. Mg/Ca-Based Paleotemperature Records

The Mg/Ca record of Core MD98-2172 extends back to ~158 ka (the base of studied interval, at ~24 m). Figure 4a shows the SSTs record derived from the Mg/Ca ratio of *G. ruber*. Core-top Mg/Ca SST is 27.8°C, which is close to the annual mean SST of 28.4°C observed today. The SST varies between 22.7 and 29.7°C, with an average value of 26.2°C. The lower SSTs occur during the glacial periods, with an average of 25.0 and 25.6°C within MIS 2–4 and late MIS 6, respectively. The higher SSTs are found during interglacial periods, with averages of 28.0 and 27.0°C within MIS 1 and MIS 5, respectively.

The TWTs of Core MD98-2172 are based on the *P. obliquolata* Mg/Ca record (Figure 4b). Today, the positions of the 18°C isotherm in the Timor Sea and on the equatorial 90°E Ridge are all at a water depth of ~150 m where water temperature changes most rapidly and is therefore used to define the depth of the thermocline (DOT) (http://odv.awi.de). Core-top Mg/Ca-based TWT is 21.9°C, which higher than the TWT recorded today. The TWT varies between 18.9 and 26.1°C, with an average of 21.8°C. The respective mean TWTs of 21.3 and 21.7°C within MIS 2–4 and late MIS 6 are lower than those during interglacial periods, that is, 23.2 and 21.8°C for MIS 1 and MIS 5, respectively.

The Mg/Ca record of Core MD77-150 extends back to ~103 ka (the base of the studied interval at ~2.19 m). The average SST in the lower part of the Holocene (note that the upper 6 Kyr are missing) is 27.6°C, which is very close to the modern annual mean of 27.5°C (Figure 4a). The reconstructed SST varies between 23.5 and 28.5°C, with a mean of 25.3°C. The average SSTs are 27.6, 24.9, and 25.4°C during the early MIS 1, MIS 2–4, and MIS 5a–5d respectively, that is, they are higher within interglacial periods than during the glacial period.

The TWT variations in Core MD77-150 follow those of SST with a clear glacial–interglacial oscillation (Figure 4), albeit with less pronounced amplitudes. The reconstructed TWTs vary between 19.9 and 25.3°C, with an average value of 21.5°C. The mean TWT for the early Holocene is 23.5°C. The lower TWT occurs during MIS 2–4, with an average of 21.3°C, while higher TWTs are found during interglacial periods, with mean values of 23.5 and 21.4°C within early MIS 1 and MIS 5a–5d, respectively.

The SSTs of Core MD77-150 exhibit lower values than those of Core MD98-2172 during the late MIS 5, but their relative changes are coherent since the end of MIS 5. However, the change in TWT for MD77-150 has followed that of Core MD98-2172 since late MIS 5.

### 5.3. Thermocline Depth

The differences in Mg/Ca-based temperature between the surface-dwelling species *G. ruber* and the thermocline-dwelling species *P. obliquiloculata* have been used as an indicator of past changes in the DOT (Anand et al., 2003; Holbourn et al., 2011; Xu et al., 2006). An increase of the vertical thermal gradient ($\Delta T_{(G.\ ruber\text{-}P.\ obliquiloculata)}$, abbreviated as $\Delta T$) has been interpreted as a shallowing of the DOT, and vice versa (Dang et al., 2012; Xu et al., 2006).

The evolution of $\Delta T$ in Core MD98-2172 exhibits glacial–interglacial oscillations (Figure 4c). It varies between 1.3 and 7.6°C, with a mean of 4.4°C. The value of $\Delta T$ increases during interglacials, with averages of 4.8 and 5.2°C for MIS 1 and MIS 5, respectively, but drops to 3.7 and 3.9°C within MIS 2–4 and during MIS 6, respectively. This implies that the thermocline was shallower during interglacials than during the glacial intervals in the Timor Sea. The exception is that $\Delta T$ in MIS 5e is also low, which is close to MIS 6.

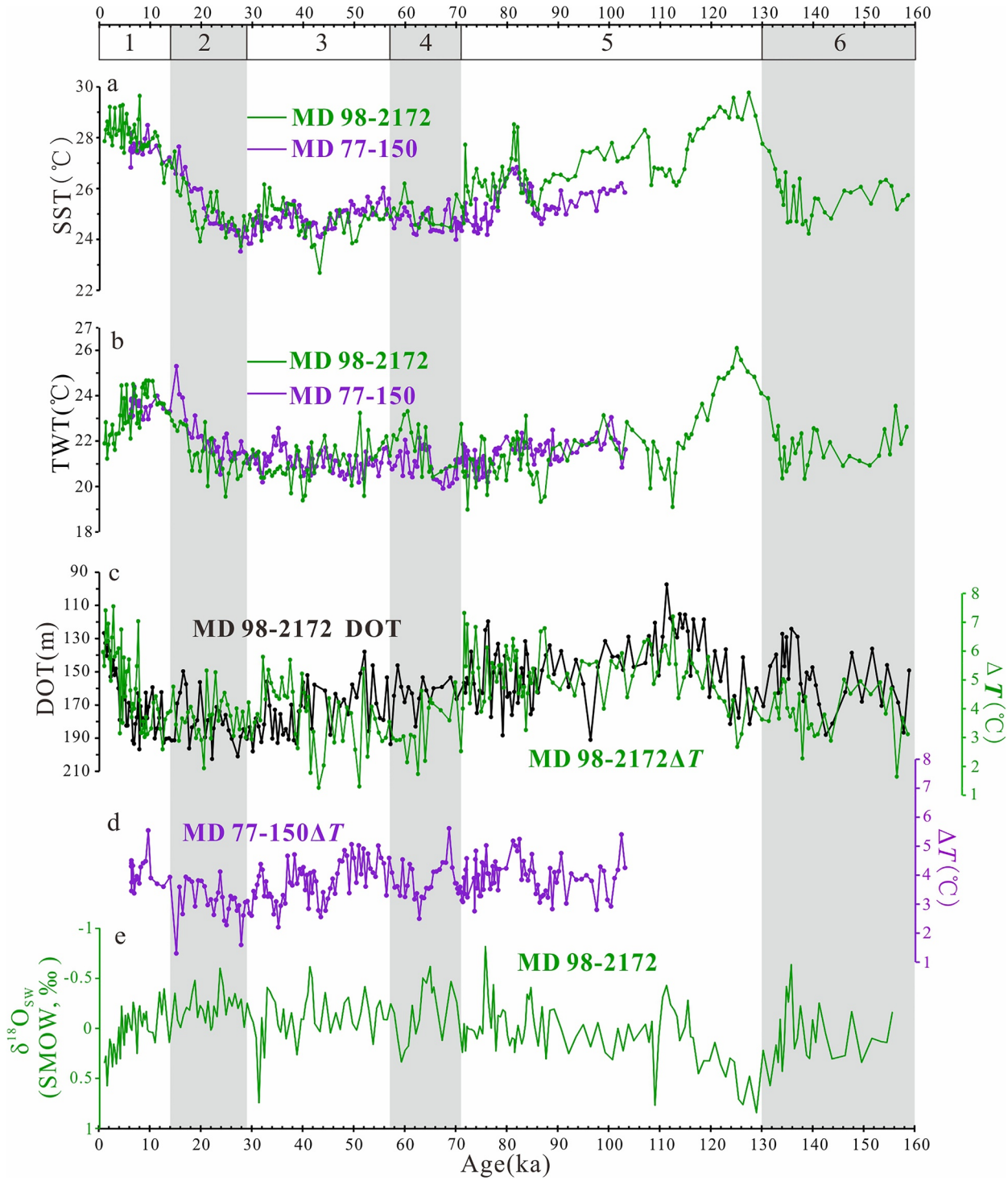


**Figure 4.** (a) *Globigerinoides ruber* Mg/Ca sea surface temperature (SST) of Core MD98-2172 and Core MD77-150; (b) *Pulleniatina obliquiloculata* Mg/Ca thermocline water temperature (TWT) of Core MD98-2172 and Core MD77-150; (c) the thermocline depth (DOT) based on the transport function of planktonic foraminifera (black) and $\Delta T$ (The temperature differences between *G. ruber* and *P. obliquiloculata*) (green) of Core MD98-2172; (d) $\Delta T_{(G.\ ruber\text{-}P.\ obliquiloculata)}$ of Core MD77-150; (e) surface seawater $\delta^{18}O_{sw}$ corrected for ice volume of Core MD98-2172.

Planktonic foraminiferal census data have also been used to estimate the DOT with the transfer function developed by Andreasen and Ravelo (1997) for the tropical Pacific Ocean. For Core MD98-2172, the estimated DOT values exhibit trends similar to those of $\Delta T$. The DOT varies between 97 and 203 m, with an average value of 162 m. It is shallower during interglacials than the preceeding glacial intervals, with mean values of 168, 174, 148, and 155 m during MIS 1, MIS 2–4, MIS 5, and MIS 6, respectively (Figure 4). Similar with $\Delta T$, the DOT in MIS5e is also an exception, which is deeper and close to that of MIS 6.

The $\Delta T$ of Core MD77-150 displays consistent fluctuation with that of Core MD98-2172 but with a smaller amplitude, and it is significantly lower than Core MD98-2172 in the late MIS 5 (Figures 4c and 4d). The $\Delta T$ value of Core MD77-150 varies between 1.3 and 5.6°C, with an average value of 3.8°C. The slightly higher average $\Delta T$ of 4.1 and 3.9°C during MIS 1 and MIS 5a–d than the mean of 3.6°C during MIS 2–4 suggests a DOT shallowing during the interglacials.

### 5.4. Record of $\delta^{18}O_{sw}$ Corrected for Ice Volume Changes

The $\delta^{18}O_{sw}$ values for *G. ruber* in Core MD98-2172 vary between −0.82 and 0.84‰, with a mean of −0.02‰. The change of the $\delta^{18}O_{sw}$ values does not show obvious glacial–interglacial oscillations, with average values of −0.14 and 0.10‰ in glacial periods MIS 2–4 and late MIS 6 and 0.02 and 0.04‰ in interglacial periods MIS 1 and MIS 5. However, the $\delta^{18}O_{sw}$ values are significantly higher during early MIS 1, late MIS 3, MIS 5e, and late MIS 6 (Figure 4e).

### 5.5. The $\delta^{13}C$ Record and Paleoproductivity Indexes

The planktonic $\delta^{13}C$ value of Core MD98-2172 varies between 0.37 and 1.84‰. There is a lack of glacial–interglacial features; higher $\delta^{13}C$ values occur during MIS 1, 3, and 5a–5d and lower values are found in MIS 2, 4, 5e, and 6. The MIS 5e interval is characterized by lower planktonic $\delta^{13}C$ values compared to other warmer interglacial intervals (Figure 5e).

The relative abundances of high productivity species *Globigerina bulloides* in Core MD98-2172 vary between 2.4% and 18.0%, with an average value of 7.9%. The species relative abundances do not exhibit clear glacial–interglacial differences, with average values of 8.4% and 6.8% in MIS 2–4 and late MIS 6, and 8.3% and 7.6% in MIS 1 and MIS 5, respectively. Nonetheless, their variation trend is similar to the insolation at 30°S in December (Figures 5f and 5g).

## 6. Discussion

### 6.1. ITF Records in the East Timor Sea

Today, the main ITF flow from the Pacific to the Indian Ocean occurs within the thermocline. Since this transport of relatively cool and fresh water exceeds that of warm surface waters, the ITF cools the tropical Indian Ocean (Gordon, 2005; Gordon et al., 2003). It has been suggested that the changes from surface to thermocline dominated flow are more important to alter the stratification and surface heat fluxes of the Indian Ocean than mean ITF transport flux (Song & Gordon, 2004).

Core MD98-2172 is located in the main outflow path of the ITF in the east Timor Sea (Figure 1), therefore, is likely to record the structure and properties of water masses before the ITF enters the Indian Ocean. The changes in vertical structure of the upper water column are reflected by the DOT, which indicated the ITF transport mainly occurs within the thermocline or at the sea surface. Both fauna-based DOT proxy and the temperature difference between surface and thermocline waters ($\Delta T$) indicate that, over the last 160 Kyr, the thermocline was deeper during the glacial intervals (MIS 2–4 and MIS 6) than during the interglacial intervals (MIS 1 and MIS 5) at the site of Core MD98-2172 (Figure 4). One can interpret the deepening of the thermocline during the glacial intervals as resulting from the decrease in mean ITF intensity and an increase in surface ITF relative to thermocline flux.

However, previous studies of cores from Northwest Australia showed that the paleoproductivity fluctuations in the Timor Sea were strongly influenced by monsoonal wind patterns (Holbourn et al., 2005; Xu et al., 2006). The strength of the NW monsoon influences the upper water column in the Timor Sea by intensifying vertical

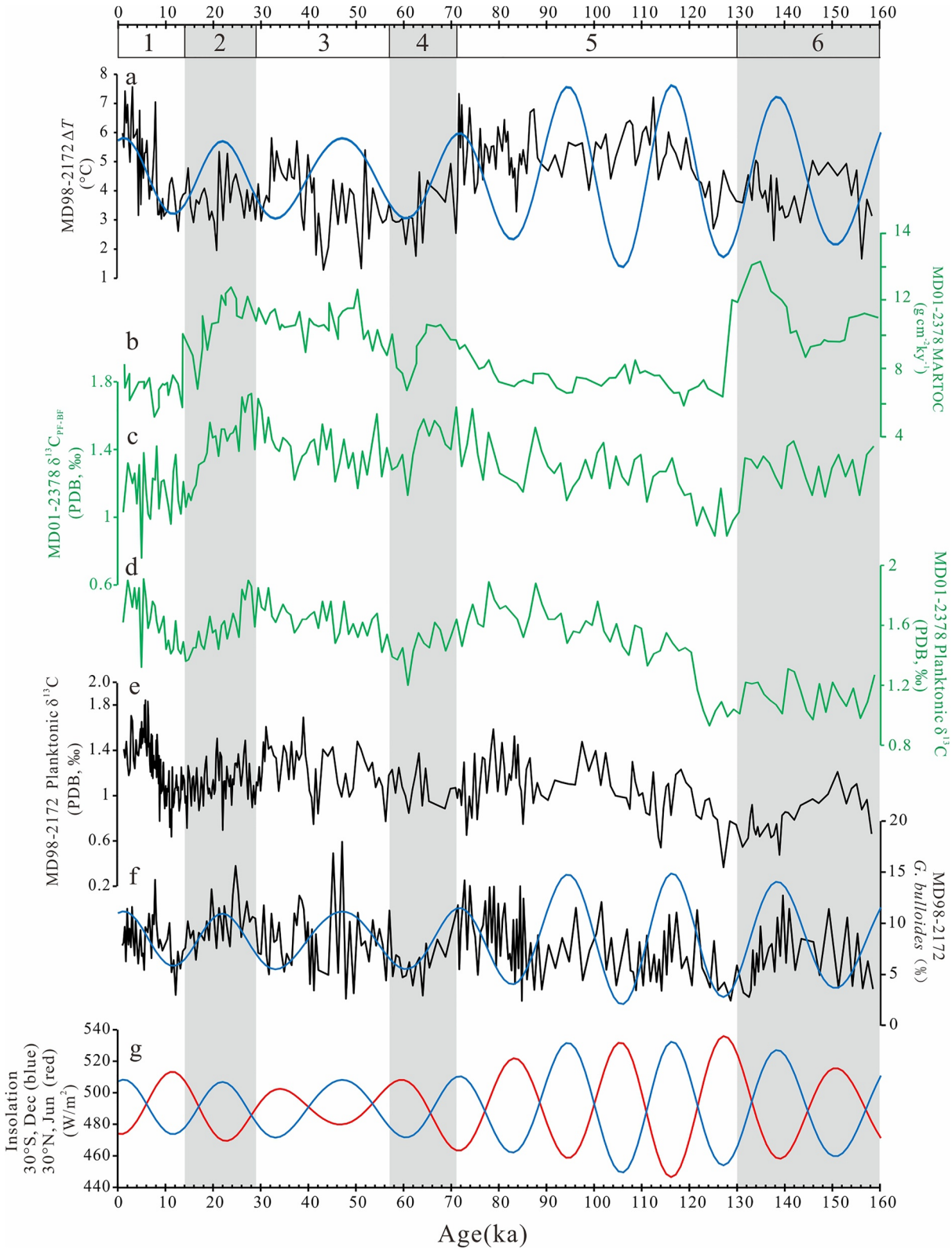


**Figure 5.** (a) $\Delta T$ (black) of Core MD98-2172 and insolation at 30°S in December (blue); (b) total organic carbon accumulation rates (MARTOC) of MD 01-2378 (Holbourn et al., 2005); (c) $\Delta\delta^{13}C_{PF\text{-}BF}$ of MD 01-2378 (Holbourn et al., 2005); (d) planktonic $\delta^{13}C$ of MD 01-2378 (Holbourn et al., 2005); (e) planktonic $\delta^{13}C$ of MD98-2172; (f) the relative abundance of *Globigerina bulloides* of MD98-2172 and insolation at 30°S in December (blue); (g) insolation at 30°S in December (blue) and at 30°N in June (red).

mixing of the surface layer during December–February (Xu et al., 2006). Therefore, the shallow DOT may not be only caused by the stronger thermocline ITF, but may also be affected by monsoon-related vertical mixing of the surface layer.

The evolution of primary production in the Timor Sea was reconstructed over the last 460 Kyr through a multiple-proxy study of Core MD01-2378 (Holbourn et al., 2005), adjacent to Core MD98-2172. The planktonic $\delta^{13}C$ data of Core MD98-2172 exhibit similar variations to those of Core MD01-2378 (Figure 5). The $\delta^{13}C_{PF\text{-}BF}$ value, which is frequently used for qualitative estimation of export productivity in the tropical and subtropical oceans (Jian et al., 2001; Sarnthein & Winn, 1990), and the total organic carbon (TOC) accumulation rates of Core MD01-2378 indicate that, on a glacial–interglacial timescale, the paleoproductivity in the Timor Sea was higher in the glacial periods than in the interglacial periods over the last 160 Kyr (Holbourn et al., 2005). However, those productivity maxima during glacial periods occur when the thermocline depth was deeper rather than shallower at the site of Core MD98-2172 (Figures 4 and 5). Previous research suggested that the higher productivity during the Last Glacial Maximum in the Timor Sea may have been driven by a reduction of warm, low-salinity surface currents, resulting in a shallower thermocline and the development of weak upwelling (Holbourn et al., 2005; Müller & Opdyke, 2000). Here we consider a different scenario. The deep thermocline in the glacial reconstructed from Core MD98-2172 rules out the proposition that primary productivity responded to the vertical structure of the water column. We suggest that the glacial productivity maxima resulted from an increased supply of terrigenous nutrients, when the sea level was low and the ITF was dominated by warm surface water transport.

Therefore, at the glacial–interglacial timescale, DOT changes in the Timor Sea may reflect the regional structure of the ITF. We propose the following scenario: as the sea levels rose to a high level during deglaciation and interglacials, fresh water from the South China Sea (SCS) which traveled through the Sunda Shelf blocked the surface ITF outflow of the Makassar Strait (refer to Figure 1c), hence intensifying the thermocline ITF flow and resulting in a shallower DOT. During the glacial periods when the sea level was low, the Sunda Shelf was exposed, low-salinity surface water from the SCS cannot enter the southern Makassar Strait, therefore, allowing a stronger advection of the surface ITF flow from the Makassar Strait, with a relatively weaker thermocline flow. This would result in a deepening of the DOT.

By comparing the $\Delta T$ and the insolation variation curve, we find that the DOT of Core MD98-2172 exhibits a distinct precession periodicity in interglacial periods MIS 1 and MIS 5, especially at 70–90 ka and 110–130 ka for MIS 5 (Figure 5a). When December insolation at 30°S is high, the thermocline becomes shallower, and vice versa (Figure 5a). The modern ITF is affected by semiannual monsoonal shifts; during the NW monsoon, ITF is dominated by the cold thermocline flux (Gordon, 2005; Gordon et al., 2003). During the interglacials associated with peak 30°S in December insolation, the NW monsoon strengthens and causes heavy rains; large amount of fresh water can flow from the SCS into the Java Sea (Ardi et al., 2020). This fresh surface water is advected into the southern Makassar Strait, blocking the warm surface ITF flux and making it possible for the thermocline ITF to become dominant (shallower DOT).

The abundances of *G. bulloides* are high in mid- to high-latitude regions, but the species is also common in upwelling areas and boundary currents in low-latitude regions where surface productivity is high (Fairbanks et al., 1982; Martinez et al., 1998; Pflaumann & Jian, 1999; Thunell & Reynolds, 1984). The percentages of the high productivity species *G. bulloides* in Core MD98-2172 show no obvious glacial–interglacial cycles, while there is high coherency with the insolation at 30°S in December. The spectral analysis results of two paleoproductivity proxies planktonic $\delta^{13}C$ and *G. bulloides* % for MD98-2172 show clear precession periodicity (Figure 6), indicating that the variation of paleoproductivity in Core MD98-2172 is largely controlled by the precession with a prominent 23-Kyr cycle. This is consistent with adjacent Core MD01-2378 (Holbourn et al., 2005).

Today, there is no significant upwelling in the Timor Sea (Müller & Opdyke, 2000), where the sea surface layer is warm and with low-salinity during the moist NW monsoon period (Figure 2). The blockage of warm surface ITF due to the strengthened NW monsoon could lead to the thermocline to shoal in the Timor Sea, which would promote local upwelling of nutrient-rich Indian Ocean intermediate water (Xu et al., 2006). A similar scenario should appear during the interglacial period of high sea level due to the intensified NW monsoon when insolation at 30°S in December increased, which would result in increased productivity as well as content of high productivity species *G. bulloides* in Core MD98-2172. During the glacial period of low sea level, the strengthened NW monsoon could bring more terrigenous nutrients, resulting in increased productivity.

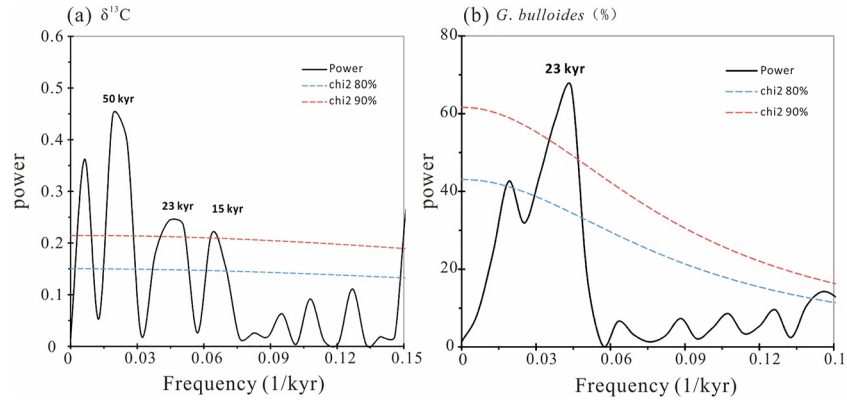


**Figure 6.** Spectra of (a) planktonic $\delta^{13}C$ and (b) *Globigerina bulloides* % for MD98-2172. Spectral analyses were performed using REDFIT (Schulz & Mudelsee, 2002). Dashed lines denote 90% (red) and 80% (blue) confidence levels.

In summary, in the Timor Sea, the glacial-interglacial changes from a surface- to thermocline-dominated ITF likely reflect a sea-level control on the geometry of the pathways within the Indonesian seas, and in particular the connection with the SCS. During the interglacial period of high sea level, the ITF structure reflects long-term changes in the monsoonal activity controlled by the precession periodicity, whose effect can be observed today on a seasonal basis. How will such a change be manifested in the heat transport processes of the ITF?

### 6.2. Glacial–Interglacial Changes of SST Gradient Along the ITF Pathway

The reconstructed SST changes of Core MD98-2172 from the east Timor Sea and Core MD77-150 from the 90°E Ridge of the Indian Ocean show clear glacial–interglacial patterns over the last 160 Kyr (Figure 4). The SSTs in the east Timor Sea and above the 90°E Ridge were similar during MIS 2–4 as well as during the early part of MIS 1, while SSTs were markedly warmer in the east Timor Sea during the later part of interglacial MIS 5.

The two cores are both located in the main outflow pathway of the ITF in the eastern Indian Ocean. To understand the heat transport processes of the ITF from the western Pacific to the eastern Indian Ocean during the last 160 Kyr, we compared the SSTs of Core MD98-2172 and Core MD77-150 with data from Core KX97322-4 (Zhang et al., 2021) and Core MD06-3067 (Bolliet et al., 2011) in the western equatorial Pacific Ocean in the core region of the IPWP. Core MD06-3067 is located to the south of Mindanao, the main entrance area for the ITF (Figures 1 and 7, Figure S2 in Supporting Information S1).

The cleaning procedure implemented for Ma/Ca analysis for Core MD06-3067 differed from ours and Core KX97322-4 (Zhang et al., 2017), as it involved a reductive step (Bolliet et al., 2011; Martin & Lea, 2002) whereas ours and Core KX97322-4 used a nonreductive step (Barker et al., 2003). To get comparable data sets of Mg/Ca-derived temperatures, we corrected the Mg/Ca ratios of Core MD06-3067 for partial dissolution induced by the reductive cleaning following the methods outlined by Pang et al. (2020). The conversion from Mg/Ca to temperature for Core KX97322-4 (Zhang et al., 2021) is different from our method. It uses the equation developed by Hollstein et al. (2017): $Mg/Ca = 0.26e^{0.097T}$, while we used the equation from Anand et al. (2003). The Mg/Ca-temperature calibration of Hollstein et al. (2017) is based on regional studies of modern surface sediments in the Western Pacific Warm Pool. Yet, since the resulting regression lines for *G. ruber* match the regressions published by Anand et al. (2003), we kept the original temperature data of KX97322-4 for comparison.

The SST records of cores MD98-2172, MD06-3067 and KX97322-4 all exhibit clear glacial–interglacial cycles. Their SST values are similar during the interglacial period, but the SST of Core KX97322-4 and Core MD06-3067 are higher than that of Core MD98-2172 during MIS 2–4 (Figure 7, Figure S2 in Supporting Information S1). The SST differences between cores KX97322-4 from the western equatorial Pacific Ocean (WEP for KX97322-4), MD06-3067 from Mindanao (Min for MD06-3067) and Core MD98-2172 from Timor Sea (Tim for MD98-2172) ($\Delta SST_{WEP-Tim}$ and $\Delta SST_{Min-Tim}$) were smaller during the interglacial periods (with averages of 1.4 and 0.9°C in MIS 1 and MIS 5 for $\Delta SST_{WEP-Tim}$ and 1.0 and 1.0°C in MIS 1 and MIS 5 for $\Delta SST_{Min-Tim}$, respectively) but increased during the glacial periods (with averages of 2.5 and 2.2°C in MIS 2–4 and MIS 6 for $\Delta SST_{WEP-Tim}$, and 1.8 and 1.9°C in MIS 2–4 and MIS 6 for $\Delta SST_{Min-Tim}$, respectively) (Figure 7, Figure S2 in Supporting Information S1).

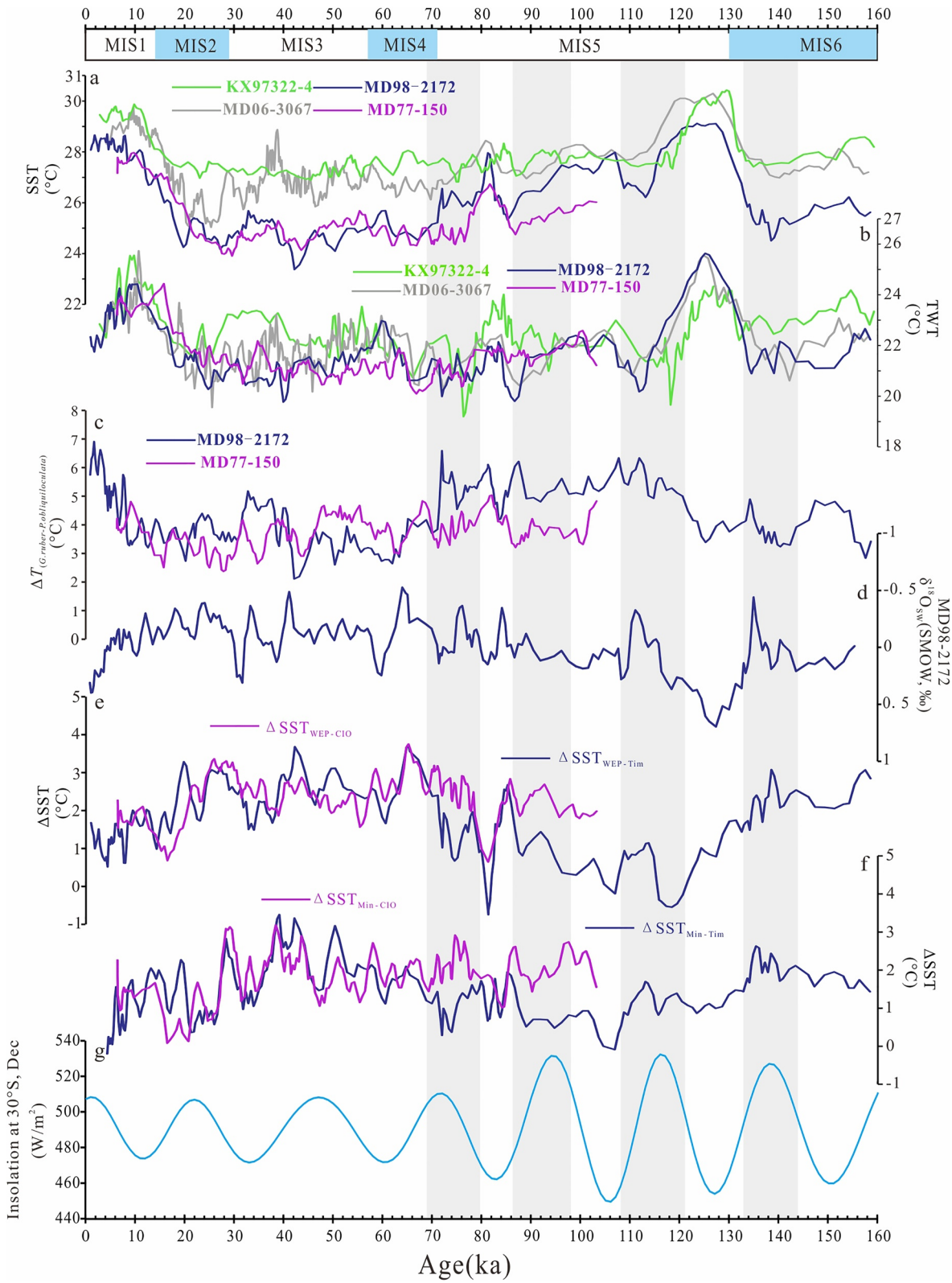


**Figure 7.** (a) Three points moving average sea surface temperatures (SSTs) of cores MD98-2172, MD77-150, MD06-3067 (Bolliet et al., 2011) and KX97322-4 (Zhang et al., 2021); (b) Three points moving average thermocline water temperatures (TWTs) of cores MD98-2172, MD77-150, MD06-3067 (Bolliet et al., 2011) and KX97322-4 (Zhang et al., 2021); (c) Three points moving average $\Delta T$ of cores MD98-2172 and MD77-150; (d) Three points moving average $\delta^{18}O_{sw}$ of Core MD98-2172; (e) Three points moving average $\Delta SST_{WEP-CIO}$ and $\Delta SST_{WEP-Tim}$; (f) Three points moving average $\Delta SST_{Min-CIO}$ and $\Delta SST_{Min-Tim}$; (g) Insolation at 30°S in December. Gray shadings mark the high insolation stages at 30°S in December.

By comparing the data of Mg/Ca-based SST changes of the cores in the central equatorial Indian Ocean (SK157 GC04) and the central equatorial Pacific Ocean (ODP 871) with the cores in westernmost margin (SK 237 GC09) and south (GeoB 10038-4) of the IPWP (Figure 1), Saraswat et al. (2019) reconstructed the spatial extent and intensity of the IPWP and suggested a considerable decrease in the warm pool extent during MIS 6 as well as during the last glacial interval. Xu et al. (2006, 2010) also indicated the expansion or intensification of the IPWP during early interglaciation. Therefore, we interpret the larger $\Delta SST_{WEP-Tim}$ and $\Delta SST_{Min-Tim}$ during the glacials (MIS 6 and MIS 2–4) than the interglacials (MIS 5) as likely resulting from the shrinking IPWP during the glacial periods.

However, a comparison of SSTs from Core MD77-150 with those from cores KX97322-4 and MD06-3067 in the western equatorial Pacific Ocean reveals a strikingly different scenario from that for Core MD98-2172. With the exception of the Termination I, the SSTs of the core from 90°E Ridge were lower than those in the western equatorial Pacific Ocean since the late MIS 5 (Figure 7, Figure S2 in Supporting Information S1). The calculated SST gradients between cores KX97322-4 and MD06-3067 from the western equatorial Pacific Ocean and the core MD77-150 from the 90°E Ridge of central Indian Ocean (CIO for MD77-150) ($\Delta SST_{WEP-CIO}$ and $\Delta SST_{Min-CIO}$) are different from $\Delta SST_{WEP-Tim}$ and $\Delta SST_{Min-Tim}$. The $\Delta SST_{WEP-CIO}$ and $\Delta SST_{Min-CIO}$ values in late MIS 5 (with averages of 2.2 and 2.0°C, respectively) were close to those in the subsequent glacial periods (MIS 2–4) (with an averages of 2.5°C for $\Delta SST_{WEP-CIO}$ and 1.7°C for $\Delta SST_{Min-CIO,}$ respectively) (Figure 7, Figure S2 in Supporting Information S1). Core MD77-150 is located along the southern margin of the IPWP where modern SST is obviously affected by the intensity and extent of the IPWP (Figures 1 and 2). The above results indicate that, the variation of the IPWP extent between interglacial and glacial periods is difficult to explain the changes of SST gradient between the equatorial 90°E Ridge and the central IPWP since the late MIS 5.

The present-day SST changes over the equatorial 90°E Ridge are not affected by upwelling intensity and/or the lateral advection of colder waters from western Sumatra during the SE monsoon (Figure 2). As Core MD77-150 is located along the main outflow path of the ITF in the eastern Indian Ocean, was the change of the SST gradient between the equatorial 90°E Ridge and the central IPWP affected by the heat transport processes of the ITF in the geological past?

### 6.3. ITF Heat Transport to the Eastern Indian Ocean

As shown in Figure 7b, the Mg/Ca-derived TWT records obtained on *P. obliquiloculata* exhibit similar changes in Core MD06-3067, which lies to the south of Mindanao (ITF main entrance area) and in cores MD98-2172 and MD77-150 located along the main outflow path of the ITF in the eastern Indian Ocean. They resemble the TWT record of the Core KX97322-4 based on the *Neogloboquadrina dutertrei* Mg/Ca record (Zhang et al., 2021). Several previous studies showed that the western equatorial Pacific thermocline water originates from the basin-wide shallow overturning circulation of the Pacific Ocean, which is fed by the subduction of relatively salty, warm surface waters in the subtropical North and South Pacific (Dang et al., 2020; Jian et al., 2022; Lo et al., 2022; Zhang et al., 2021). However, they didn't discuss how the thermocline water gets into the Indian Ocean. Our results suggest that the ITF is likely to be an important route for thermocline water transport from the equatorial western Pacific into the Indian Ocean since 160 ka.

#### 6.3.1. ITF Heat Transport on the Glacial–Interglacial Time Scale

Consistent with what is observed in the record of Core MD98-2172, the $\Delta T$ value of Core MD77-150, located along the SEC in the main outflow of the ITF, also reveals a deeper thermocline during the last glacial intervals (MIS 2–4) than during the interglacial intervals of late MIS 5 and early MIS 1 (Figures 4d and 7c), although the amplitude of $\Delta T$ is not as large as for Core MD98-2172. These results suggest that the structural evolution of the thermocline at the site of Core MD77-150 on the 90°E Ridge was controlled by changes in the ITF structure, as recorded in the upstream site MD98-2172 in the heart of the ITF, within the Timor Sea. This confirms the consistency of the structure and character of the ITF after entering the Indian Ocean.

Due to the shrinkage of the IPWP during the glacial periods (Saraswat et al., 2019; Xu et al., 2006, 2010), the $\Delta SST_{Min-Tim}$ and $\Delta SST_{WEP-Tim}$ were larger during the glacials (MIS 2–4 and MIS 6) than during the interglacials (MIS 1 and MIS 5) (Figure 7). However, $\Delta SST_{WEP-CIO}$ and $\Delta SST_{Min-CIO}$ did not show similar trends, but with the larger SST difference between the western equatorial Pacific Ocean and the 90°E Ridge during late MIS 5 (Figure 7, Figure S2 in Supporting Information S1). We suggest that this is due to the intensified thermocline ITF during the interglacial periods with more cold thermocline water into the eastern Indian Ocean. Some of the ITF water entering the tropical Indian Ocean will first upwell to the surface before spreading southward within

the surface Ekman layer (Gordon, 2005), which could cause the SST of Core MD77-150 to drop, leading to an increase of $\Delta SST_{WEP-CIO}$ and $\Delta SST_{Min-CIO}$, as observed during late MIS 5 (Figure 7).

By contrast, during the glacial periods, the ITF flowed as a surface current although the thermocline ITF was weakened. We interpret this as resulting from the strengthening of the surface ITF and weakening thermocline ITF, which transported more warm surface water and less cold thermocline water into the eastern Indian Ocean. This explains the similarity in SST at the two sites of MD98-2172 and MD77-150 during MIS 2–4 (Figure 7).

#### 6.3.2. Precession Modulation of ITF Heat Transport During MIS 5

Figure 7 shows that, during 69–80 ka and 86–98 ka of MIS 5, $\Delta SST_{WEP-CIO}$ and $\Delta SST_{Min-CIO}$ were larger than $\Delta SST_{WEP-Tim}$ and $\Delta SST_{Min-Tim}$, respectively, and that the thermocline of Core MD98-2172 was shallower during these two intervals. Nevertheless, during 80–86 ka, $\Delta SST_{WEP-CIO}$ and $\Delta SST_{Min-CIO}$ were very close to $\Delta SST_{WEP-Tim}$ and $\Delta SST_{Min-Tim}$, respectively, with a deeper thermocline of MD98-2172 and MD77-150 at the same time.

Although the 90°E Ridge record does not extend into the early MIS 5, the data from Core MD98-2172 do suggest that in the 108–121 ka interval the thermocline in the Timor Sea was shallow, and SSTs were lower than at the sites of cores MD06-3067 (Bolliet et al., 2011) and KX97322-4 (Zhang et al., 2021) from the central IPWP. This was accompanied by the decrease in the SSS of MD98-2172 indicated by $\delta^{18}O_{sw}$ (Figure 7d). In the 98–108 ka and 121–132 ka intervals, the thermocline at the site of Core MD98-2172 was deeper than during the 108–121 ka interval and the SST was more similar to the other two cores from the central IPWP. The link between higher SSS and deeper thermocline at the site of Core MD98-2172 is particularly clear during the interval of 121–132 ka.

When insolation at 30°S in December was high during the three intervals of 69–80 ka, 86–98 ka and 108–121 ka within the last interglacial, the intensified NW monsoon resulted in increased rainfall and fresh water input, which formed fresh water obstruction in Makassar Strait and enhanced the thermocline ITF. The thermocline ITF brought cold and low salinity water into the eastern Indian Ocean. When some of such water upwell to the surface (Gordon, 2005), it could result in a drop in SST of cores MD77-150 and MD98-2172, especially for MD77-150 which was influenced by the gradually cooling SEC along its route (as seen in Figures 1 and 2a). Consequently, the SST difference between MD77-150 and sites in the central IPWP was increased in the intervals of 69–80 ka and 86–98 ka, and so were those between MD98-2172 and sites in the central IPWP during 108–121 ka (Figure 7).

In addition, during the intervals of 69–80 ka and 86–98 ka, $\Delta T$ indicated deeper thermocline depth at Core MD77-150 than Core MD98-2172 (Figure 7). This may be caused by the weakening of thermocline ITF in the central Indian Ocean; when the cold thermocline ITF is transported into the eastern Indian Ocean, part of the thermocline water could enter the mixed layer gradually through the upward turbulent activity with the increasing distance from the ITF source.

By contrast, during 80–86 ka, 98–108 ka, and 121–132 ka when insolation at 30°S in December was decreased (Figure 7), the SE monsoon would intensify (Ardi et al., 2020). This could enhance the surface ITF, which brought warm surface water into the eastern Indian Ocean, resulting in a rise in the SST of cores MD77-150 and MD98-2172. Therefore, the SST difference between Core MD77-150 and those in the central IPWP was decreased during 80–86 ka (Figure 7). During the 121–132 ka (Termination II to early MIS 5e), the DOT of Core MD98-2172 reached its deepest position within MIS 5, and was even deeper than that at the end of MIS 6, which was also seen at Core MD01-2378 from Timor Sea (Xu et al., 2006, 2008). The deeper DOT and higher SSS of Core MD98-2172 point to the strengthened warm surface ITF. This probably stemmed from the rapidly rising sea level combined with the enhanced SE monsoon during Termination II. This also caused a drop in the SST difference between Core MD98-2172 and cores in the central IPWP (Figure 7).

## 7. Conclusions

Two cores (Core MD98-2172 located at the main outflow path of the ITF in the Timor Sea and Core MD77-150 located on the 90°E Ridge in the equatorial Indian Ocean) have been investigated. By reconstructing past changes of SST and TWT at these two sites and paleoproductivity of MD98-2172, and comparing with two cores from the central IPWP, we have illustrated the role of the ITF in regulating the heat transport processes during the last 160 Kyr in the Indo-Pacific region.

The SST difference between the central IPWP and the east Timor Sea increased during the glacial periods and decreased during the interglacial period, indicating that the reduced extent and weakened intensity of the IPWP

during glacial period. However, the SST difference between the central IPWP and the 90°E Ridge in MIS 5 was close to those in the subsequent glacial periods.

The changes from surface to thermocline dominated ITF were influenced by the glacial–interglacial sea-level changes, as well as by the monsoonal activity. The thermocline structure changes in the equatorial 90°E Ridge and the east Timor Sea are similar, which confirms the consistency in the vertical profile of the ITF after its entry into the Indian Ocean. The TWT in the equatorial western Pacific and eastern Indian Ocean presents similar change trend along the ITF pathway, indicating that the ITF is likely to be an important route for thermocline water transport from the equatorial western Pacific into the Indian Ocean during the last 160 Kyr.

During the interglacial periods, the intensified thermocline ITF input more cold thermocline water to the eastern Indian Ocean, causing the SST of Core MD77-150 to drop. By contrast, the intensification of the surface ITF during the glacial periods brought more warm surface water into the eastern Indian Ocean, which resulted in a SST difference between the central region of the IPWP and the equatorial 90°E Ridge in the glacial period similar to that in the interglacial periods.

During the last interglacial period of high sea level, when insolation at 30°S in December increased, the NW monsoon intensified, and the thermocline ITF brought cold and low salinity thermocline water into the eastern Indian Ocean. When insolation at 30°S in December decreased, the SE monsoon intensified, and the enhanced surface ITF brought warm surface water into the eastern Indian Ocean.

## Data Availability Statement

The new data presented in this study are available in the figshare database (Ding et al., 2023).

**Acknowledgments**
This work was supported by the National Natural Science Foundation of China (41376056), the Research on paleo-climate in the eastern Indian Ocean (GASI-04-01-03) and Foreign Cultural and Educational Experts Employment Program (GDW20181100256). We also acknowledge the constructive comments of three anonymous reviewers that helped to improve the manuscript.

## References

Anand, P., Elderfield, H., & Conte, M. (2003). Calibration of Mg/Ca thermometry in planktonic foraminifera from a sediment trap time series. *Paleoceanography*, *18*(2), 1050. https://doi.org/10.1029/2002PA000846

Andreasen, D. J., & Ravelo, A. C. (1997). Tropical Pacific Ocean thermocline depth reconstructions for the last glacial maximum. *Paleoceanography*, *12*(3), 395–413. https://doi.org/10.1029/97pa00822

Ardi, R. D. W., Aswan, Maryunani, K. A., Yulianto, E., Putra, P. S., Nugroho, S. H., & Istiana (2020). Last deglaciation–Holocene Australian-Indonesian monsoon rainfall changes off southwest Sumba, Indonesia. *Atmosphere*, *11*(9), 932. https://doi.org/10.3390/atmos11090932

Barker, S., Greaves, M., & Elderfield, H. (2003). A study of cleaning procedures used for foraminiferal Mg/Ca paleothermometry. *Geochemistry, Geophysics, Geosystems*, *4*(9), n/a. https://doi.org/10.1029/2003GC000559

Bemis, B. E., Spero, H. J., Bijma, J., & Lea, D. W. (1998). Reevaluation of the oxygen isotopic composition of planktonic foraminifera: Experimental results and revised paleotemperature equations. *Paleoceanography*, *13*(2), 150–160. https://doi.org/10.1029/98pa00070

Bolliet, T., Holbourn, A., Kuhnt, W., Laj, C., Kissel, C., Beaufort, L., et al. (2011). Mindanao Dome variability over the last 160 kyr: Episodic glacial cooling of the West Pacific Warm Pool. *Paleoceanography*, *26*(1), PA1208. https://doi.org/10.1029/2010PA001966

Bray, N. A., Hautala, S., Chong, J., & Pariwono, J. (1996). Large-scale sea level, thermocline, and wind variations in the Indonesian Throughflow region. *Journal of Geophysical Research*, *101*(C5), 12239–12254. https://doi.org/10.1029/96jc00080

Dang, H., Jian, Z., Bassinot, F., Qiao, P., & Cheng, X. (2012). Decoupled Holocene variability in surface and thermocline water temperatures of the Indo-Pacific Warm Pool. *Geophysical Research Letters*, *39*(1), L01701. https://doi.org/10.1029/2011GL050154

Dang, H., Jian, Z., Wang, Y., Mohtadi, M., Rosenthal, Y., Ye, L., et al. (2020). Pacific warm pool subsurface heat sequestration modulated Walker circulation and ENSO activity during the Holocene. *Science Advances*, *6*(42), eabc0402. https://doi.org/10.1126/sciadv.abc0402

de Villiers, S., Greaves, M., & Elderfield, H. (2002). An intensity ratio calibration method for the accurate determination of Mg/Ca and Sr/Ca of marine carbonates by ICP-AES. *Geochemistry, Geophysics, Geosystems*, *3*(1), 1525–2027. https://doi.org/10.1029/2001GC000169

Ding, X., Bassinot, F., Guichard, F., & Fang, N. Q. (2013). Indonesian Throughflow and monsoon activity records in the Timor Sea since the last glacial maximum. *Marine Micropaleontology*, *101*, 115–126. https://doi.org/10.1016/j.marmicro.2013.02.003

Ding, X., Bassinot, F., Pang, X. L., Kou, Y. X., & Zhou, L. P. (2023). Oxygen and carbon isotopes, Mg/Ca ratios and depth of thermocline data for the last 160 kyr in the eastern Indian Ocean [Dataset]. Figshare. https://doi.org/10.6084/m9.figshare.23160137

Fairbanks, R. G., Sverdlove, M., Free, R., Wiebe, P. H., & Bé, A. W. H. (1982). Vertical distribution and isotopic fractionation on living planktonic foraminifera from the Panama Basin. *Nature*, *198*(5877), 841–844. https://doi.org/10.1038/298841a0

Fan, W., Jian, Z., Bassinot, F., & Chu, Z. (2013). Holocene centennial-scale changes of the Indonesian and South China Sea Throughflows: Evidences from the Makassar Strait. *Global and Planetary Change*, *111*, 111–117. https://doi.org/10.1016/j.gloplacha.2013.08.017

Fan, W., Jian, Z., Chu, Z., Dang, H., Wang, Y., Bassinot, F., et al. (2018). Variability of the Indonesian Throughflow in the Makassar Strait over the last 30 ka. *Scientific Reports*, *8*(1), 5678. https://doi.org/10.1038/s41598-018-24055-1

Gordon, A. L. (1986). Interocean exchange of thermocline water. *Journal of Geophysical Research*, *91*(C4), 5037–5046. https://doi.org/10.1029/jc091ic04p05037

Gordon, A. L. (2005). Oceanography of the Indonesian Seas and their Throughflow. *Oceanography*, *18*(4), 14–27. https://doi.org/10.5670/oceanog.2005.01

Gordon, A. L., Dwi Susanto, R., & Vranes, K. (2003). Cool Indonesian Throughflow as a consequence of restricted surface layer flow. *Nature*, *425*(6960), 824–828. https://doi.org/10.1038/nature02038

Gordon, A. L., & Fine, R. A. (1996). Pathways of water between the Pacific and Indian oceans in the Indonesian seas. *Nature*, *379*(6561), 146–149. https://doi.org/10.1038/379146a0

Gordon, A. L., Huber, B. A., Joseph Metzger, E., Dwi Susanto, R., Hurlburt, H. E., & Rameyo Adi, T. (2012). South China Sea Throughflow impact on the Indonesian Throughflow. *Geophysical Research Letters*, *39*(11), L11602. https://doi.org/10.1029/2012GL052021

He, Y., & Wang, H. (2021). Terrestrial material input to the northwest shelf of Australia through the Pliocene-Pleistocene period and its implications on continental climates. *Geophysical Research Letters*, *48*(17), e2021GL092745. https://doi.org/10.1029/2021GL092745

Hirst, A. C., & Godfrey, J. S. (1993). The role of Indonesian Throughflow in a global ocean GCM. *Journal of Physical Oceanography*, *23*(6), 1057–1086. https://doi.org/10.1175/1520-0485(1993)023<1057:troiti>2.0.co;2

Holbourn, A., Kuhnt, W., Kawamura, H., Jian, Z., Grootes, P., Erlenkeuser, H., & Xu, J. (2005). Orbitally paced paleoproductivity variations in the Timor Sea and Indonesian Throughflow variability during the last 460 kyr. *Paleoceanography*, *20*(3), PA3002. https://doi.org/10.1029/2004PA001094

Holbourn, A., Kuhnt, W., & Xu, J. (2011). Indonesian Throughflow variability during the last 140 ka: The Timor Sea outflow. *Geological Society, London, Special Publications*, *355*(1), 283–303. https://doi.org/10.1144/SP355.14

Hollstein, M., Mohtadi, M., Rosenthal, Y., Sanchez, P. M., Oppo, D., Mendez, G. M., et al. (2017). Stable oxygen isotopes and Mg/Ca in planktic foraminifera from modern surface sediments of the Western Pacific Warm Pool: Implications for thermocline reconstructions. *Paleoceanography*, *32*(11), 1174–1194. https://doi.org/10.1002/2017PA003122

Huang, E., Tian, J., & Liu, J. (2015). Dynamics of the Australian-Indonesian monsoon across termination II: Implications of molecular-biomarker reconstructions from the Timor Sea. *Palaeogeography, Palaeoclimatology, Palaeoecology*, *423*, 32–43. https://doi.org/10.1016/j.palaeo.2015.01.027

Jian, Z., Huang, B., Kuhnt, W., & Lin, H. (2001). Late Quaternary upwelling intensity and east Asian monsoon forcing in the South China Sea. *Quaternary Research*, *55*(3), 363–370. https://doi.org/10.1006/qres.2001.2231

Jian, Z., Wang, Y., Dang, H., Mohtadi, M., Rosenthal, Y., Lea, D. W., et al. (2022). Warm pool ocean heat content regulates ocean–continent moisture transport. *Nature*, *612*(7938), 92–99. https://doi.org/10.1038/s41586-022-05302-y

Linsley, B. K., Rosenthal, Y., & Oppo, D. W. (2010). Holocene evolution of the Indonesian Throughflow and the western Pacific warm pool. *Nature Geoscience*, *3*(8), 578–583. https://doi.org/10.1038/ngeo920

Lisiecki, L. E., & Raymo, M. E. (2005). A Pliocene-Pleistocene stack of 57 globally distributed benthic $\delta^{18}O$ records. *Paleoceanography*, *20*(1), PA1003. https://doi.org/10.1029/2004PA001071

Lo, L., Shen, C. C., Zeeden, C., Tsai, Y. H., Yin, Q., Yang, C. C., et al. (2022). Orbital control on the thermocline structure during the past 568 kyr in the Solomon Sea, southwest equatorial Pacific. *Quaternary Science Reviews*, *295*, 107756. https://doi.org/10.1016/j.quascirev.2022.107756

Lückge, A., Mohtadi, M., Rühlemann, C., Scheeder, G., Vink, A., Reinhardt, L., & Wiedicke, M. (2009). Monsoon versus ocean circulation controls on paleoenvironmental conditions off southern Sumatra during the past 300,000 years. *Paleoceanography*, *24*(1), PA1208. https://doi.org/10.1029/2008PA001627

Martin, P. A., & Lea, D. W. (2002). A simple evaluation of cleaning procedures on fossil benthic foraminiferal Mg/Ca. *Geochemistry, Geophysics, Geosystems*, *3*(10), 8401. https://doi.org/10.1029/2001GC000280

Martinez, J. I., Taylor, L., De Deckker, P., & Barrows, T. T. (1998). Planktonic foraminifera from the eastern Indian Ocean: Distribution and ecology in relation to the Western Pacific Warm Pool (WPWP). *Marine Micropaleontology*, *34*(3–4), 121–151. https://doi.org/10.1016/s0377-8398(97)00045-5

Mohtadi, M., Lückge, A., Steinke, S., Groeneveld, J., Hebbeln, D., & Westphal, N. (2010). Late Pleistocene surface and thermocline conditions of the eastern tropical Indian Ocean. *Quaternary Science Reviews*, *29*(7–8), 887–896. https://doi.org/10.1016/j.quascirev.2009.12.006

Müller, A., & Opdyke, B. N. (2000). Glacial-interglacial changes in nutrient utilization and paleoproductivity in the Indonesian Throughflow sensitive Timor Trough, easternmost Indian Ocean. *Paleocenography*, *15*(1), 85–94. https://doi.org/10.1029/1999pa900046

Oppo, D. W., & Rosenthal, Y. (2010). The Great Indo-Pacific communicator. *Science*, *328*(5985), 1492–1494. https://doi.org/10.1126/science.1187273

Paillard, D., Laberyrie, L., & Yiou, P. (1996). Macintosh program performs time-series analysis. *Eos, Transactions American Geophysical Union*, *77*(39), 379. https://doi.org/10.1029/96EO00259

Pang, X., Bassinot, F., & Sepulcre, S. (2020). Cleaning method impact on the Mg/Ca of three planktonic foraminifera species: A downcore study along a depth transect. *Chemical Geology*, *549*, 119690. https://doi.org/10.1016/j.chemgeo.2020.119690

Pflaumann, U., & Jian, Z. (1999). Modern distribution patterns of planktonic foraminifera in the South China Sea and western Pacific: A new transport technique to estimate regional sea-surface temperatures. *Marine Geology*, *156*(1–4), 41–83. https://doi.org/10.1016/s0025-3227(98)00173-x

Saraswat, R., Singha, D. P., Leab, D. W., Mackensenc, A., & Naikd, D. K. (2019). Indonesian Throughflow controlled the westward extent of the Indo-Pacific Warm Pool during glacial-interglacial intervals. *Global and Planetary Change*, *183*, 103031. https://doi.org/10.1016/j.gloplacha.2019.103031

Sarnthein, M., & Winn, K. (1990). Reconstruction of low and middle latitude export productivity, 30,000 years B. P. to present: Implication for control of global carbon reservoirs. In M. E. Schlesinger (Ed.), *Climate-ocean interaction* (pp. 319–342). Springer.

Schulz, M., & Mudelsee, M. (2002). REDFIT: Estimating red-noise spectra directly from unevenly spaced paleoclimatic time series. *Computers & Geosciences*, *28*(3), 421–426. https://doi.org/10.1016/s0098-3004(01)00044-9

Smith, R. A., Castañeda, I. S., Groeneveld, J., De Vleeschouwer, D., Henderiks, J., Christensen, B. A., et al. (2020). Plio-Pleistocene Indonesian Throughflow variability drove eastern Indian Ocean sea surface temperatures. *Paleoceanography and Paleoclimatology*, *35*(10), e2020PA003872. https://doi.org/10.1029/2020PA003872

Song, Q., & Gordon, A. L. (2004). Significance of the vertical profile of the Indonesian Throughflow transport to the Indian Ocean. *Geophysical Research Letters*, *31*(16), L16307. https://doi.org/10.1029/2004GL02360

Song, Q., Gordon, A. L., & Visbeck, M. (2004). Spreading of the Indonesian Throughflow in the Indian Ocean. *Journal of Physical Oceanography*, *34*(4), 772–792. https://doi.org/10.1175/1520-0485(2004)034<0772:sotiti>2.0.co;2

Spooner, M. I., Barrows, T. T., De Deckker, P., & Paterne, M. (2005). Palaeoceanography of the Banda Sea, and Late Pleistocene initiation of the northwest monsoon. *Global and Planetary Chang*, *49*(1–2), 28–46. https://doi.org/10.1016/j.gloplacha.2005.05.002

Sprintall, J., Wijffels, S. E., Molcard, R., & Jaya, I. (2009). Direct estimates of the Indonesian Throughflow entering the Indian Ocean: 2004–2006. *Journal of Geophysical Research*, *114*(C7), C07001. https://doi.org/10.1029/2008JC005257

Stuiver, M., & Braziunas, T. F. (1993). Modeling atmospheric $^{14}C$ influences and $^{14}C$ ages of marine samples to 10,000 BC. *Radiocarbon*, *35*(1), 137–189. https://doi.org/10.1017/s0033822200013874

Thunell, R. C., & Reynolds, L. A. (1984). Sedimentation of planktonic foraminifera: Seasonal changes in species flux in the Panama Basin. *Micropaleontology*, *30*(3), 243–262. https://doi.org/10.2307/1485688

Tozuka, T., Qu, T., Masumoto, Y., & Yamagata, T. (2009). Impacts of the South China Sea Throughflow on seasonal and interannual variations of the Indonesian Throughflow. *Dynamics of Atmospheres and Oceans*, *47*(1–3), 73–85. https://doi.org/10.1016/j.dynatmoce.2008.09.001

Waelbroeck, C., Labeyrie, L., Michel, E., Duplessy, J. C., McManus, J. F., Lambeck, K., et al. (2002). Sea-level and deep water temperature changes derived from benthic foraminifera isotopic records. *Quaternary Science Reviews*, *21*(1–3), 295–305. https://doi.org/10.1016/s0277-3791(01)00101-9

Wang, B., Liu, J., Kim, H. J., Webster, P. J., & Yim, S. Y. (2012). Recent change of the global monsoon precipitation (1979–2008). *Climate Dynamics*, *39*(5), 1123–1135. https://doi.org/10.1007/s00382-011-1266-z

Webster, P., Magana, V., Palmer, T., Shukla, J., Tomas, R., Yanai, M., & Yasunari, T. (1998). Monsoons: Processes, predictability, and the prospects for prediction. *Journal of Geophysical Research*, *103*(C7), 14451–14510. https://doi.org/10.1029/97jc02719

Xu, J., Holbourn, A., Kuhnt, W., Jian, Z., & Kawamura, H. (2008). Changes in the thermocline structure of the Indonesian outflow during Terminations I and II. *Earth and Planetary Science Letters*, *273*(1–2), 152–162. https://doi.org/10.1016/j.epsl.2008.06.029

Xu, J., Kuhnt, W., Holbourn, A., Andersen, & N., & Bartoli, G. (2006). Changes in the vertical profile of the Indonesian Throughflow during Termination II: Evidence from the Timor Sea. *Paleoceanography*, *21*(4), PA4202. https://doi.org/10.1029/2006PA001278

Xu, J., Kuhnt, W., Holbourn, A., Regenberg, M., & Andersen, N. (2010). Indo-Pacific warm pool variability during the Holocene and Last Glacial Maximum. *Paleoceanography*, *25*(4), PA4230. https://doi.org/10.1029/2010PA001934

Zhang, S., Li, T. G., Chang, F. M., Yu, Z. F., Xiong, Z. F., & Wang, H. X. (2017). Correspondence between the ENSO-like state and glacial-interglacial condition during the past 360 kyr. *Chinese Journal of Oceanology and Limnology*, *35*(5), 1018–1031. https://doi.org/10.1007/s00343-07-6082-9

Zhang, S., Yu, Z. F., Gong, X., Wang, Y., Chang, F. M., Lohmman, G., et al. (2021). Precession cycles of the El Niño/South Oscillation-like system controlled by Pacific upper-ocean stratification. *Communications Earth & Environment*, *2*, 239. https://doi.org/10.1038/s43247-021-00305-5